PHYSICAL REVIEW E **66**, 056203 (2002)

Phase synchronization in coupled chaotic oscillators with time delay

J. Y. Chen and K. W. Wong
Department of Computer Engineering and Information Technology, City University of Hong Kong, Hong Kong, China

J. W. Shuai
Department of Physics and Astronomy, Ohio University, Athens, Ohio 45701

(Received 23 October 2001; revised manuscript received 2 July 2002; published 21 November 2002)

The phase synchronization (PS) of two Rössler oscillators with time-delayed signal coupling is studied. We find that time delay can always lead to PS even when the delay is very long. Moreover, with the increase of time delay, the coupling strength at the transition to PS undergoes a nearly periodic wave distribution. At some fixed time-delayed signal coupling, a PS region is followed by a non-PS region when the coupling strength increases. However, an increase of the coupling leads to the PS state again. This phenomenon occurs in systems with a relatively large PS transition point.

DOI: 10.1103/PhysRevE.66.056203 PACS number(s): 05.45.−a

I. INTRODUCTION

Systems with time-delayed feedback signals are quite ubiquitous in nature. The delay is usually caused by finite signal transmission speed and memory effect. There have been extensive investigations on the influence of time-delayed feedback (including synchronization and amplitude death) in the context of coupled limit cycle oscillator systems [1]. It has been found that time delay has a significant effect on the characteristics of all the major cooperative phenomena such as frequency locking and phase drift [2]. As many chaotic models developed in physics, chemistry, and biology are formulated in terms of coupled nonlinear oscillators [3], time delay also plays an important role in the control and synchronization of these chaotic oscillators. It has been reported that a delayed feedback on one of the system variables can control the stabilization of the unstable periodic orbits of chaotic dynamics [4]. In a coupled time-delayed system, complete synchronization can be obtained and applied to communication [5]. The observation of lag synchronization also characterizes constant time delay between two signals [6].

Recently, the notion of synchronization has been extended to phase synchronization (PS) in a system composed of two mutually coupled nonidentical self-sustained chaotic oscillators [7]. PS in coupled chaotic system is analogous to the phase locking of periodic oscillators, where the locking itself is the only concern. For a certain coupling strength, phase locking can be observed for two chaotic oscillators while their amplitudes remain chaotic and weakly correlated [8]. This phenomenon has found applications in laboratory experiments such as lasers [9], circuits [10], and plasmas [11], as well as natural systems such as the extended ecological system [12], magnetoencephalographic activity of Parkinsonian patients [13], electrosensitive cells of the paddlefish, Canadian lynx-hare populations [14], and solar activity [15].

As time delay is generally encountered in signal transmission, it is important to study the characteristics of PS with time delay. A major advantage of delay coupling is that systems separated by a variety of distances can still be synchronized using the phase, even when the signal transmission is slow. Similar to other kinds of physical phenomena with time delay, PS with time delay is also important in engineering and physiological systems, where signal transmission and delayed feedback dynamics play a crucial role [16]. For example, in arrays of semiconductor lasers, synchronizing the lasing elements in phase is of importance in order to obtain a large output power concentrated in a single-lobed far field pattern [17]. The synchronization of arrays of semiconductor lasers by global coupling with time delay has been demonstrated by experiments [18]. In particular, the phase-locked oscillator is found important in the understanding of neural information processing [19]. The investigation of motivated time delay may improve such models. However, in spite of a large body of evidence of PS with time delay in nature, the study of PS phenomenon in a system coupling with time-delay signals is not yet available.

In this paper we show that PS can be obtained with coupling sets at various time delays. With the increase of time delay, a nearly periodic wave distribution of PS transition points is found. At small PS transitions that correspond to the valley of the wave, the PS phenomena are the same as those of traditional coupling with no time delay, where only the unique PS transition is found. However, at large transitions that are near the peak of the wave, there can be two types of PS transitions. One of them is a *local* PS (LPS) transition while the other is a *global* PS (GPS) transition. We characterize the final PS transition as a GPS transition where phase locking is always maintained even at an increase of coupling strength. In contrast to this, the LPS transition refers to the early transition to PS but then non-PS is observed again at an increased coupling strength. Our simulation results show that time-delayed signal coupling may lead to some special properties of PS that are in contrast to the situation without time delay.

II. GLOBAL PHASE SYNCHRONIZATION

We start with two coupled nonidentical Rössler systems [20], describing the evolution of three-dimensional vectors:

$$\dot{x}_{1,2} = -\omega_{1,2} y_{1,2} - z_{1,2} + \epsilon [x_{2,1}(t-\tau) - x_{1,2}],$$

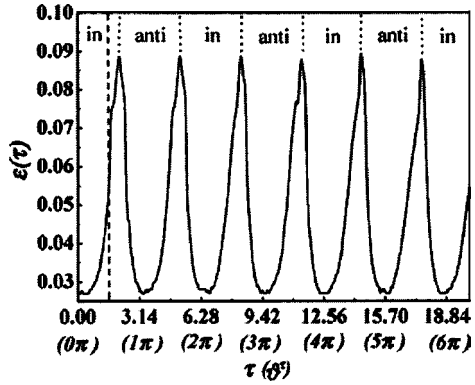

FIG. 1. The GPS transition $\epsilon_c(\tau)$ at various delays of coupled signals τ. In this example, the delay phase difference $\vartheta^\tau \approx \tau$ as $\omega_0 = 1$. The dashed line shows the position where $\vartheta^\tau = \pi/2$, while the dotted line figures out two types of regions that are in-correlated and anticorrelated, respectively. They appear between one another regularly.

$$\dot{y}_{1,2} = \omega_{1,2} x_{1,2} + a y_{1,2}, \tag{1}$$

$$\dot{z}_{1,2} = f + z_{1,2}(x_{1,2} - c),$$

where dots denote temporal derivatives, τ is time delay, ϵ represents the coupling strength, and $\omega_{1,2} = \omega_0 \pm \Delta$ (Δ being the frequency mismatch between the two chaotic oscillators). We set $a = 0.165$, $f = 0.2$, and $c = 10$ so as to make the system generate chaotic dynamics. In what follows we focus our study on the case $\omega_0 = 1$ and $\Delta = 0.015$. When the attractor is oriented so that its projection on the plane (x_i, y_i) exhibits a phase flow circulating the origin, this is the phase coherent attractor. Its phase can be conveniently introduced as

$$\phi_i = \tan^{-1}[y_i(t)/x_i(t)] \quad \text{with} \quad i = 1,2. \tag{2}$$

Here the value of $\tan^{-1}$ is taken to be such that ϕ_1 and ϕ_2 are continuous in time, i.e., they have no 2π jumps as t varies. With this convention, ϕ_i increases continuously with t for orbits at the chaotic attractors. The mean frequency of ϕ_i can be obtained using the formula $\Omega_i = \langle \dot{\phi}_i \rangle$. If $\tau = 0$, the case becomes directional coupling which has been investigated extensively [7,8,21,22]. As ϵ increases under this situation, the system identifies subsequent transitions from nonsynchronization to GPS. The GPS transition is a function of τ, denoted as $\epsilon_c(\tau)$. With the increase of τ, $\epsilon_c(\tau)$ is regular and nearly periodic, as observed in Fig. 1. We find that $\tau = 0$ is just one of the positions where $\epsilon_c(\tau)$ is a local minimum. In our simulation, Eq. (1) is numerically solved using a fourth-order Runge-Kutta method with time step $= 0.002$, the time length of calculation is 4000 after omitting the initial time length of 4000. These simulation settings are used throughout this paper. After simulations with smaller time steps, longer lengths of calculation and initial time, we found that the above conditions are accurate enough to make the simulation results free from computational accuracy.

It is necessary to investigate the relationship between $\epsilon_c(\tau)$ and τ as they appear quite regularly. In Eqs. (1), the delay signals between $x_i(t)$ and $x_i(t-\tau)$ contain the delay phase difference

$$\vartheta_i^\tau = \tan^{-1}\frac{y_i(t)}{x_i(t)} - \tan^{-1}\frac{y_i(t-\tau)}{x_i(t-\tau)} = \phi_i(t) - \phi_i(t-\tau) \quad \text{with} \quad i = 1,2 \tag{3}$$

from the attractors on the (x_i, y_i) plane. Although the two systems in Eqs. (1) are nonidentical, they have the same mean frequency $\Omega \approx \omega_0$ after PS [7]. As a result, the mean delay phase difference $\langle \vartheta^\tau \rangle$ after the PS transition can be approximately characterized as

$$\langle \vartheta_1^\tau \rangle \approx \langle \vartheta_2^\tau \rangle \approx \omega_0 \tau. \tag{4}$$

In the following, we simply denote $\vartheta^\tau = \omega_0 \tau$.

To develop an approximate theory of PS with different time delays in Eqs. (1), we rewrite it in terms of (A_i, ϕ_i, z_i) variables, where $A_i = \sqrt{x_i^2 + y_i^2}$ is the amplitude,

$$\dot{A}_{1,2} = a A_{1,2} \sin^2 \phi_{1,2} - z_{1,2} \cos \phi_{1,2} + \epsilon [A_{2,1}(t-\tau) \times \cos(\phi_{2,1} - \vartheta_{2,1}^\tau) \cos \phi_{1,2} - A_{1,2} \cos^2 \phi_{1,2}],$$

$$\dot{\phi}_{1,2} = \omega_{1,2} + a \sin \phi_{1,2} \cos \phi_{1,2} + z_{1,2}/A_{1,2} \sin \phi_{1,2} - \epsilon [A_{2,1}(t-\tau)/A_{1,2} \cos(\phi_{2,1} - \vartheta_{2,1}^\tau) \sin \phi_{1,2} - \cos \phi_{1,2} \sin \phi_{1,2}],$$

$$\dot{z}_{1,2} = f - c z_{1,2} + A_{1,2} z_{1,2} \cos \phi_{1,2}. \tag{5}$$

Substituting $\phi_i = \omega_0 t + \theta_i$ into the equations for $\dot{\phi}_{1,2}$, averaging the equations over the period $2\pi/\omega_0$ to eliminate some terms, and then subtracting two slow phases with phase difference $\theta = \theta_1 - \theta_2$, we have

$$\frac{d\theta}{dt} = 2\Delta - \frac{\epsilon K^+}{2} \sin \theta \cos \vartheta^\tau - \frac{\epsilon K^-}{2} \cos \theta \sin \vartheta^\tau, \tag{6}$$

where

$$K^+ = \left(\frac{A_2(t-\tau)}{A_1} + \frac{A_1(t-\tau)}{A_2} \right) \tag{7}$$

and

$$K^- = \left(\frac{A_2(t-\tau)}{A_1} - \frac{A_1(t-\tau)}{A_2} \right). \tag{8}$$

The process of getting Eq. (6) from Eqs. (5) at $\tau = 0$ has been discussed by other researchers in order to obtain a qualitative estimate of $\epsilon_c(0)$ [6]. We extend the process to a variety of time delay. It is difficult to estimate the exact value of $\epsilon_c(\tau)$ at different τ. However, we can find the approximate values for some special cases. In the following, we analyze two special cases in detail.

If $\vartheta^\tau = n\pi$ ($n = 0,1,2,3,...$), Eq. (6) can be transformed into

$$\theta = \arcsin \frac{4\Delta}{\epsilon K^+}. \tag{9}$$

In another special case where $\vartheta^\tau = (2n+1)\pi/2$, Eq. (6) can be written as

$$\theta = \arccos \frac{4\Delta}{\epsilon K^-}. \tag{10}$$

Comparing Eqs. (9) and (10), it is evident that the PS transition in Eq. (10) is much larger than that in Eq. (9) because $K^- < K^+$. Furthermore, when ϑ^τ transforms from $n\pi$ to $(2n+1)\pi/2$, the factors that mainly determine the value of $\epsilon_c(\tau)$ change continuously from Eq. (9) to Eq. (10). By this means, when we neglect the nonlinear dynamics of $\sin\vartheta$ ($\cos\vartheta$) and amplitude fluctuations, we can make a coarse approximation between the two special cases and the local extreme points shown in Fig. 1. This figure shows that the PS transition in Eq. (9) corresponds to the local minimum transition i.e., $\epsilon_c^{\min} = \epsilon_c(\tau)|_{\vartheta^\tau = n\pi}$, and that of Eq. (10) corresponds to the value near the local maximum transition, i.e., $\epsilon_c^{\max} = \epsilon_c(\tau)|_{\vartheta^\tau=(2n+1)\pi/2}$. Here, $\tau = \vartheta^\tau/\omega_0$, as obtained from Eq. (4). In our example, the values of both τ and ϑ^τ are identical because $\omega_0 = 1$. If we select $\omega_0 \neq 1$, the local minimum and maximum points still locate near $\vartheta^\tau = n\pi$ and $(2n+1)\pi/2$, respectively. However, $\tau \neq \vartheta^\tau$ in this case. In Fig. 1, it is found that the values of $\epsilon_c^{\min}$ are approximately constant at various time delays. Moreover, they are around the positions where $\vartheta^\tau \approx n\pi$ as estimated from Eq. (9). On the other hand, the values of $\epsilon_c^{\max}$ also have similar maximum values at various time delays. Their positions are near $\vartheta^\tau = (2n+1)\pi/2$, as found from Eq. (10). The dotted line marked in Fig. 1 indicates a clear mismatch between the time delay $\pi/2$ and $\epsilon_c^{\max}$. This is mainly because the value of K^- is sensitive to the amplitude fluctuations, while we neglect the factor in the above analysis.

We try to figure out the PS transition at local minimum (maximum) points from both Eqs. (6)–(10) and the simulation results. We take a local minimum point, i.e., $\vartheta^\tau = 3\pi$ as an example. The evolution of K^+ at $\epsilon = 0.0$ and 0.03 is shown in Figs. 2(a) and 2(b), respectively. In Fig. 2(a), the average value is 2.45, as marked by a horizontal line. In Fig. 2(b), $\langle K^+ \rangle = 2.16$, which is close to the stable value 2.0. Therefore this case has a fixed point and the PS transition point can be estimated as $\epsilon_c^{\min}(\tau) \approx 2\Delta$ with $\langle K^+ \rangle = 2.0$ [21].

We take a maximum point in Fig. 1 with $\vartheta^\tau = 17.55$ as another example to show the evolution of K^- at $\epsilon = 0.0$ and 0.09. The point is close to $11\pi/2$ and the results are shown in Figs. 2(c) and 2(d), respectively. Comparing with Fig. 2(c), the relatively large coupling term in Fig. 2(d) enlarges the fluctuations substantially. At $\epsilon = 0.09$, $\langle K^- \rangle = 0.45$, and the maximum fluctuation of $K^-(t)$ can be 24 times larger than $\langle K^- \rangle$. Further simulation shows that in spite of the large fluctuations of $K^-(t)$ for a given ϵ and τ, the mean value $\langle K^- \rangle$ always changes substantially under different coupling strength and time delay. Thus $\langle K^- \rangle$ cannot be used to approximate the actual dynamics of $K^-(t)$.

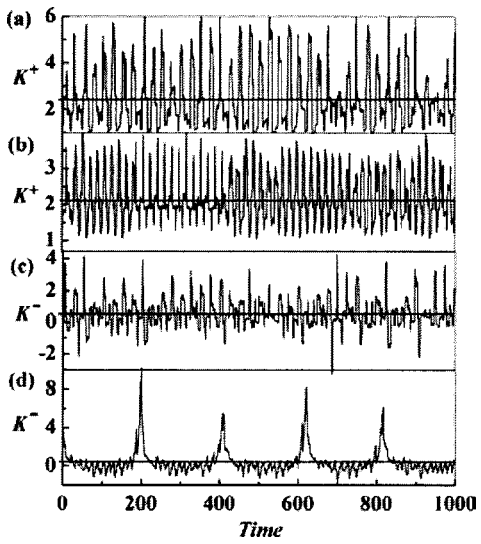

FIG. 2. (a)–(d) Time evolution of K^+ with $\tau = 9.42$ at (a) $\epsilon = 0.0$, (b) $\epsilon = 0.03$. The evolution of K^- with $\tau = 17.55$ at (c) $\epsilon = 0.0$, (d) $\epsilon = 0.09$. The horizontal lines indicate their mean values.

III. LOCAL PHASE SYNCHRONIZATION

We now study the evolution of the mean frequency difference at various values of ϵ and τ. The results of numerical simulations are plotted in Figs. 3(a)–3(d). As observed from Figs. 3(a) and 3(b), the difference of mean frequencies $\Delta\Omega$ around $\epsilon_c^{\min}$ shows similar characteristics at different time delay. Here, $\Delta\Omega$ reduces with ϵ and at last approaches zero after $\epsilon_c(\tau)$. The values of the GPS transition as well as the difference of mean frequencies are the same as those in the special case with $\tau = 0$ [21,23]. However, if $\epsilon_c(\tau)$ is selected around $\epsilon_c^{\max}$, the corresponding phenomena are much different, as observed in Figs. 3(c) and 3(d). In Fig. 3(c) where τ is relatively small, with the increase of ϵ, $\Delta\Omega$ reduces at first, but then begins to increase. There is a local minimum at $\epsilon \approx 0.068$, where $\Delta\Omega$ is far away from zero. Near the phase transition $\epsilon_c \approx 0.09$, $\Delta\Omega$ approaches zero rapidly. At large τ, the local minimum of $\Delta\Omega$ is not fixed and may drop to zero, as observed in Fig. 3(d). As a result, there is a small LPS region found before $\epsilon_c(\tau)$. In this example, it is in the range $\epsilon \in [0.077, 0.082]$ and $\epsilon_c \approx 0.09$.

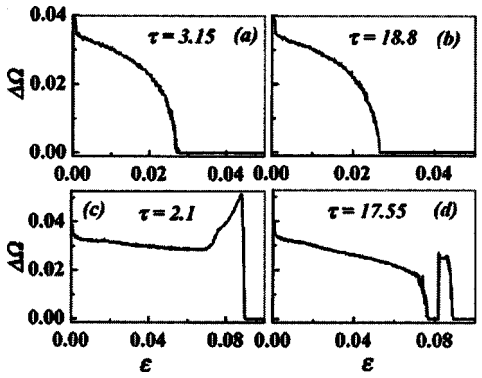

FIG. 3. (a)–(d) The difference of mean frequency $\Delta\Omega$ versus coupling strength ϵ at various time delays τ.

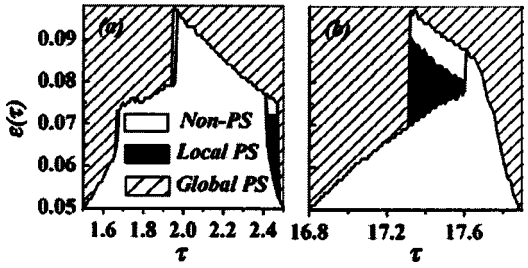

FIG. 4. (a),(b) Distribution of non-PS, local PS (LPS), and global PS (GPS) at different time delays τ.

The phenomenon of LPS can always be found around $\epsilon_c^{\max}$. As the region of LPS is very small, it is hard to be observed clearly in Fig. 1. Therefore the two peaks of $\epsilon_c(\tau)$ shown in Fig. 1 are enlarged and plotted in Figs. 4(a) and 4(b). Figure 4(a) corresponds to a small time delay while Fig. 4(b) is obtained from a comparatively large delay. A clear difference between them is the distribution of LPS. In Fig. 4(a), the LPS regions are small and distributed in several areas. However, in Fig. 4(b), they are concentrated at the top with a single and relatively large LPS region. With an increase of time delay, our simulations show that the LPS regions still concentrate at the top of the peak. However, this is not shown in this figure. If the coupling strength increases, the synchronization may change from GPS to phase locking, where the amplitudes of the two interactive oscillators have strong correlation. Notice that in the GPS regions of this figure, we did not identify the boundary between GPS and phase locking.

The distributions of non-PS, LPS, and GPS are strongly related to the nonfixed variation of the amplitudes that changes continuously with the coupling strength. In order to show the variation of amplitudes, we simulate the time evolution of x_i on the Poincaré intersection $y_i=0$ with different coupling strengths, and the results are shown in Fig. 5. In this figure, the time delay is $\tau=17.55$, i.e., the same as that chosen in Fig. 3(d). The distribution of x_i is largely affected by the value of ϵ_c. When $\epsilon<0.82$, there is a distinguished region where the points of x_2 distribute in two evident narrow bands referred to as LPS. On the other hand, a further increase of coupling strength makes the attractor of x_1 change to a broader distribution shown at $0.82<\epsilon<0.90$ in Fig. 5(a), while the attractor of x_2 remains coherent. This region corresponds to the non-PS part in Fig. 3(d). After $\epsilon \geqslant 0.9$, the attractor turns into a relatively strong coherence again and GPS is obtained.

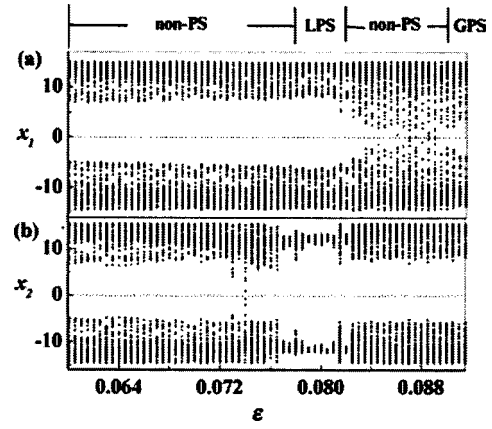

FIG. 5. (a),(b) Evolution of the variables of (a) x_1 and (b) x_2 with the coupling strength ϵ at $\tau=17.55$. Here, x_1 (x_2) is the value on the Poincaré intersection with y_1 (y_2)$=0$.

In Fig. 5, numerous points of $x_{1,2}$ are found near the zero value marked by a dotted horizontal line. However, the corresponding trajectory still mainly encircles the origin. Thus the instantaneous phase as well as the phase transition in this example can still be obtained and analyzed simply from Eq. (2). We have also employed a more general method, the Hilbert transform method [7,8], to calculate their instantaneous phases, and obtain the same results.

IV. PHASE DIFFERENCE WITH JAGGED SHAPE

In an attempt to elucidate the time evolution of phase difference before and after the PS transition, different properties are found at various time delays. Investigators have found that the 2π phase slip of θ is a distinguishing phenomenon before the GPS transition at $\tau=0$. When ϵ is far away from ϵ_c ($\epsilon<\epsilon_c$), θ increases in a nearly periodic sequence of 2π phase slips. However, when ϵ is near ϵ_c, θ increases with an intermittent sequence of 2π phase slips. After the PS transition is reached, it is basically about $\pi/2$ with a small high-frequency amplitude fluctuation [21,24,25]. However, for $\tau>0$, our simulation results show that only the region around $\epsilon_c^{\min}$ possesses these properties. In the region around $\epsilon_c^{\max}$, no distinguished scales are found. Here we do not show the simulation results of 2π phase slips that are similar to the case for $\tau=0$. For the region of large GPS transition, 2π phase slips only appear at certain ϵ. The phase difference at certain coupling strengths is shown in Figs. 6(a) and 6(b), which correspond to the time delay of Figs. 3(c) and 3(d), respectively. Let us first investigate the phase difference at coupling strength far away from ϵ_c. From Fig. 6(a), there are nearly periodic sequences of 2π phase slips at $\epsilon=0.087$. However, when $\epsilon=0.068$, which corresponds to the local minimum point of $\Delta\Omega$ in Fig. 3(c), θ increases linearly. No 2π phase slips can be found although its mean frequency difference is evidently smaller. For ϵ near the GPS transition, an irregular jagged shape for θ is observed. An example is given in Fig. 6(a) with $\epsilon=0.0895$. At $\epsilon=0.09$, GPS is obtained and θ fluctuates only slightly. However, the fluctuation is also in jagged shape. Similarly, Fig. 6(b) shows that θ increases with an irregular jagged shape at a value near ϵ_c, e.g., $\epsilon=0.088$. At a value far away from ϵ_c, i.e., near the LPS transition, 2π phase slips are found. They are shown by the curves corresponding to $\epsilon=0.073$ and 0.085. As there is a LPS region before the GPS transition, θ in this region and in the region after the GPS transition are plotted in the lower part of Fig. 6(b). The solid line shows θ in the LPS region at $\epsilon=0.08$ while the dotted line corresponds to that after the GPS transition. We find that the fluctuation of θ in the former case is similar to the phenomenon when $\tau=0$ [21,24]. Moreover, the jagged fluctuation of θ (dotted line) is just the same as that in Fig. 6(a). Evidently, in regions just before and after

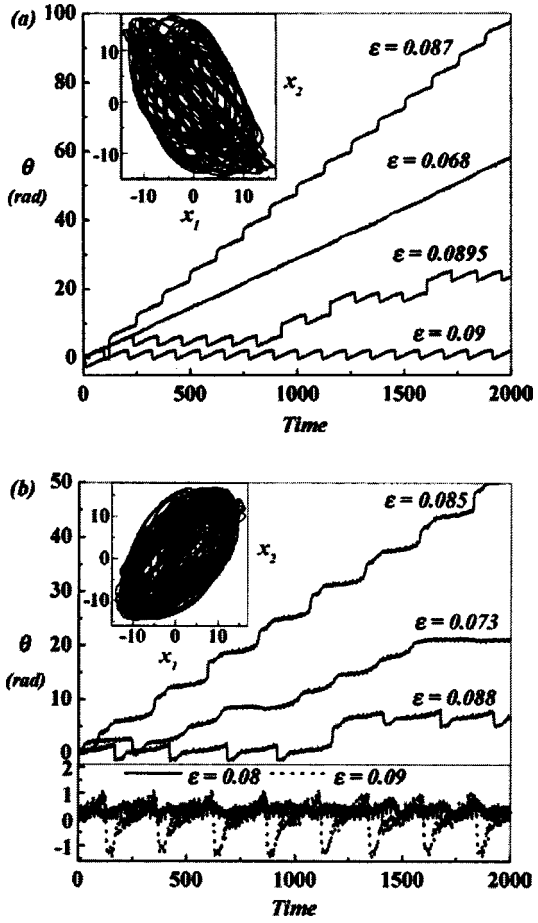

FIG. 6. Time evolutions of phase difference θ in a system of two coupled Rössler attractors at various values of coupling strength ϵ and delay time τ. The time delay is (a) $\tau=2.1$ and (b) $\tau=17.55$. They are the same as Figs. 3(c) and 3(d), respectively. The inner plots are projections of the attractor on the plane $(x_1(t),x_2(t))$, which show a relatively weak correlation between signals $x_1(t)$ and $x_2(t)$.

the GPS transitions that are around $\epsilon_c^{\max}$, the θ sequence always appears jagged shape. This phenomenon cannot be found in the region with the LPS transition.

From Eq. (6), we find that the time evolution of θ is influenced by ϑ^τ. In order to observe the evolution of ϑ^τ with the increase of $\epsilon(\tau)$, it is plotted at three different coupling strengths 0.08, 0.088, and 0.09 in Figs. 7(a)–7(c) when $\tau=17.55$. At LPS where $\epsilon=0.08$, the distribution of ϑ^τ is stable with noise fluctuation, while at $\epsilon=0.088$ and 0.09, the distribution of ϑ^τ has occasional jumps. Evidently, the jagged shapes of θ in Fig. 6(b) correspond to the irregular jumps of ϑ^τ. When ϑ^τ appears as a stable value with noise fluctuation, as shown in Fig. 7(a), the corresponding θ is also stable with a small noise fluctuation, as observed in Fig. 6(b).

V. IN-CORRELATION AND ANTICORRELATION RELATIONSHIP OF INTERACTIVE SIGNALS

Although the GPS transition is quite large, the amplitudes between two interactive oscillators are still less correlated.

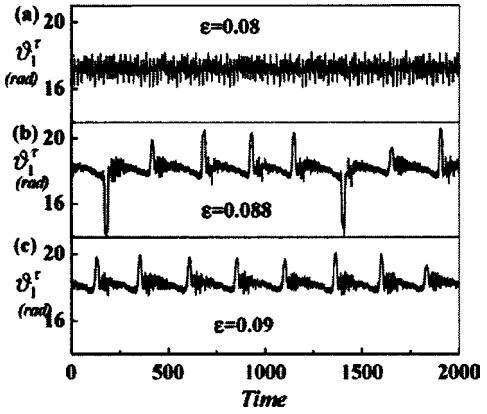

FIG. 7. (a)–(c) The time evolution of delay phase ϑ_1^τ at different coupling strengths. (a) $\epsilon(\tau)=0.08$, (b) $\epsilon(\tau)=0.088$, and (c) $\epsilon(\tau)=0.09$. The time delay is $\tau=17.55$. Notice that ϑ_2^τ has a similar portrait and is not shown here.

This is because the signals for interactive coupling have a certain time delay that reduces the correlation between $x_{1,2}(t)$ and $x_{1,2}(t-\tau)$. The inner plot of Figs. 6(a) and 6(b) are the instantaneous signals at the GPS transition $\epsilon_c=0.09$. They show that the projections of the attractors on the plane $(x_1(t),x_2(t))$ appear distorted, which indicates a relatively weak correlation between the two amplitudes. An interesting phenomenon is the unequal directions of weak correlation between x_1 and x_2. In the inner plot of Fig. 6(a), it is in-correlation where the local maxima (or minima) of $x_{1,2}$ are nearly identical. However, in the inner plot of Fig. 6(b), the two corresponding signals are weakly anticorrelated, where the local minimum of one signal corresponds to the local maximum of the other one. Further simulations show that the regions of in-correlation and anticorrelation appear in turn regularly and are divided by the local maximum of PS transitions. The regions are marked in the upper part of Fig. 1.

The in-correlation and anticorrelation of two interactive signals are caused by the coupling term in Eq. (1). We take the equation with coupling term $\epsilon[x_2(t-\tau)-x_1]$ as an example. With the increase of ϵ, the coupling term always forces the values of $x_2(t-\tau)$ and $x_1(t)$ approaching each other. By this means, they are always in-correlation after PS and can be denoted as

$$x_2(t-\tau)\uparrow \quad \text{and} \quad x_1(t)\uparrow. \tag{11}$$

On the other hand, the relationship between $x_2(t-\tau)$ and $x_2(t)$ is the same trajectory with time delay τ in a single attractor. They will appear in-correlation under the following condition:

$$x_2(t-\tau)\uparrow \quad \text{and} \quad x_2(t)\uparrow$$

$$\text{when} \quad (2n-1/2)\pi<\vartheta^\tau<(2n+1/2)\pi, \tag{12}$$

but appear in anticorrelation under the following condition:

$$x_2(t-\tau)\uparrow \quad \text{and} \quad x_2(t)\downarrow$$

$$\text{when} \quad (2n+1/2)\pi<\vartheta^\tau<(2n+3/2)\pi. \tag{13}$$

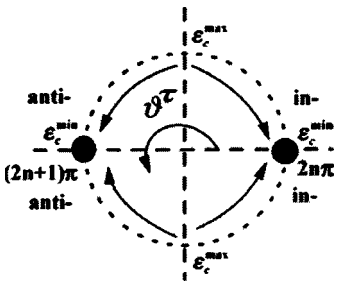

FIG. 8. The circle map transformed from Fig. 1. The two black points are the convergent points. The terms ''anti'' and ''in'' refer to anticorrelation and in-correlation, respectively, of interactive signals x_1 and x_2, while $\epsilon_c^{\min}$ and $\epsilon_c^{\max}$ are local minimum and maximum of the PS transitions.

These regular in-correlation and anticorrelation are determined by the trajectory of the Rössler attractor, which has a single rotation center. By substituting Eq. (11) into Eqs. (12) and (13), we can determine the correlation directions between $x_1(t)$ and $x_2(t)$ under different ϑ^τ. The result is just the distribution of in-correlation and anticorrelation shown in Fig. 1. Similarly, we can also take another equation with coupling term $\epsilon[x_1(t-\tau)-x_2]$ to analyze their in-correlation and anticorrelation between $x_1(t)$ and $x_2(t)$. The same result is obtained.

If we transform Fig. 1 into a circle map, the different correlating directions as well as the PS transition can be considered as the interactive results between two convergent points, as shown in Fig. 8. They correspond to $\vartheta^\tau=2n\pi$ and $(2n+1)\pi$, respectively. At the convergent points, the PS transition is a local minimum. When ϑ^τ is far away from either of them, their ϵ_c increases accordingly. At the points with $\vartheta^\tau=(2n+1)/2$, which is the farthest from the two convergent points, their ϵ_c are nearly maximum. The correlating directions of the particular ϑ^τ points are also determined by the distance from the two convergent points. When ϑ^τ approaches the left convergent point, the case results in anti-correlation. It becomes in-correlation when ϑ^τ is close to the right convergent point.

VI. CONCLUSION

In summary, we have studied the PS properties of two mutually coupled Rössler oscillators with a variety of time delay. With the increase of time delay, the GPS transition undergoes a nearly periodic sequence. Two explicit regions of the GPS transition are found. One corresponds to the transition around $\epsilon_c^{\min}$. The properties of phase difference are the same as those with zero time delay. The other region corresponds to the transition around $\epsilon_c^{\max}$. Before the GPS transition, LPS may exist. In the LPS region, the fluctuation of the phase difference is the same as that in the region with a local minimum GPS transition. However, with the increase of coupling strength, the sequence of the phase difference is quite complicated. Phase slips of 2π can only be found in certain regions of the coupling strength. Near the GPS transition, the 2π phase slips may transform to jagged slips. After GPS, the fluctuation may also appear in the jagged shape. The interaction of coupled signals appears in-correlation and anticorrelation alternately in a variety of time delays. To the best of our knowledge such results have not been reported before and they may benefit the investigation of PS in natural phenomena and complex systems.

ACKNOWLEDGMENT

The work described in this paper was fully supported by a Grant provided by CityU (Project No. 7001077).

[1] D. V. Ramana Reddy, A. Sen, and G. L. Johnston, Phys. Rev. Lett. **85**, 3381 (2000); **80**, 5109 (1998); R. Herrero, M. Figueras, J. Rius, F. Pi, and G. Orriols, *ibid.* **84**, 5312 (2000).

[2] E. Niebur, H. G. Schuster, and D. M. Kammen, Phys. Rev. Lett. **67**, 2753 (1991).

[3] R. Roy and S. Thornburg, Phys. Rev. Lett. **72**, 2009 (1994); S. K. Han, C. Kurrer, and Y. Kuramoto, *ibid.* **75**, 3190 (1995); H. U. Voss, *ibid.* **87**, 014102 (2001); in *Waves and Patterns in Chemical and Biological Media*, edited by H. L. Swinney and V. I. Krinsky (MIT, Cambridge, MA, 1992).

[4] S. Boccaletti, C. Grebogi, Y. C. Lai, H. Mancini, and D. Maza, Phys. Rep. **329**, 103 (2000); W. Just, T. Bernard, M. Ostheimer, E. Reibold, and H. Benner, Phys. Rev. Lett. **78**, 203 (1997); W. Just, D. Reckwerth, J. Möckel, E. Reibold, and H. Benner, *ibid.* **81**, 562 (1998).

[5] V. S. Udaltsov, J. P. Goedgebuer, L. Larger, and W. T. Rhodes, Phys. Rev. Lett. **86**, 1892 (2001); L. W. Liu, G. M. Ge, H. Zhao, Y. H. Wang, and G. Liang, Phys. Rev. E **62**, 7898 (2000).

[6] M. G. Rosenblum, A. S. Pikovsky, and J. Kurths, Phys. Rev. Lett. **78**, 4193 (1997); S. Boccaletti and D. L. Valladares, Phys. Rev. E **62**, 7497 (2000).

[7] M. G. Rosenblum, A. S. Pikovsky, and J. Kurths, Phys. Rev. Lett. **76**, 1804 (1996).

[8] A. S. Pikovsky, M. G. Rosenblum, G. V. Osipov, and J. Kurths, Physica D **104**, 219 (1997).

[9] E. Allaria, F. T. Arechi, A. DiGarbo, and R. Meucci, Phys. Rev. Lett. **86**, 787 (2001); E. Larinotsev, Int. J. Bifurcation Chaos Appl. Sci. Eng. **10**, 2441 (2000).

[10] U. Parlitz, L. Junge, W. Lauterborn, and L. Kocarev, Phys. Rev. E **54**, 2115 (1996); S. Taherion and Y. C. Lai, Int. J. Bifurcation Chaos Appl. Sci. Eng. **11**, 2587 (2000).

[11] C. M. Ticos, E. Rosa, Jr., W. B. Pardo, J. A. Walkenstein, and M. Monti, Phys. Rev. Lett. **85**, 2929 (2000).

[12] B. Blasius, A. Huppert, and L. Stone, Nature (London) **399**, 354 (1999).

[13] P. Tass, M. G. Rosenblum, J. Weule, J. Kurths, A. Pikovsky, J. Volmann, A. Schnitzler, and H. J. Freund, Phys. Rev. Lett. **81**, 3291 (1998).

[14] A. Neiman, X. Pei, D. Russell, W. Wojtenek, L. Wilkens, F. Moss, H. A. Braun, M. T. Huber, and K. Voigt, Phys. Rev. Lett. **82**, 660 (1999).

[15] M. Palus, J. Kurths, U. Schwarz, D. Novotna, and I. Charva-

tova, Int. J. Bifurcation Chaos Appl. Sci. Eng. **10**, 2519 (2000).
[16] *Nonlinear Analysis of Physiological Data*, edited by H. Kantz, J. Kurths, and G. Mayer-Kress (Springer, Berlin, 1998); C. W. Eurich and J. G. Milton, Phys. Rev. E **54**, 6681 (1996); P. Tass, J. Kurths, M. G. Rosenblum, G. Guasti, and H. Hefter, *ibid.* **54**, 2224 (1996).
[17] K. Otsuka and R. Kawai, Phys. Rev. Lett. **84**, 3049 (2000); J. K. Butler, D. E. Ackley, and D. Botez, Appl. Phys. Lett. **44**, 293 (1984); H. J. Yoo, J. R. Hayes, E. G. Paek, A. Scherer, and Y. S. Kwon, IEEE J. Quantum Electron. **26**, 1039 (1990).
[18] G. Kozyreff, A. G. Vladimirov, and P. Mandel, Phys. Rev. Lett. **85**, 3809 (2000).
[19] P. A. Tass, *Phase Resetting in Medicine & Biology* (Springer, Berlin, 1999); J. W. Shuai and D. M. Durand, Phys. Lett. A **264**, 289 (1999).
[20] O. E. Rössler, Phys. Lett. **57A**, 297 (1976).
[21] E. Rosa, Jr., E. Ott, and M. H. Hess, Phys. Rev. Lett. **80**, 1642 (1998); K. J. Lee, Y. Kwak, and T. K. Lim, *ibid.* **81**, 321 (1998).
[22] Z. H. Liu, Y. C. Lai, and F. C. Hoppensteadt, Phys. Rev. E **63**, 055201 (2001); Z. G. Zheng, G. Hu, and B. B. Hu, Phys. Rev. Lett. **81**, 5318 (1998).
[23] Z. G. Zheng and G. Hu, Phys. Rev. E **62**, 7882 (2000); J. Y. Chen, K. W. Wong, and J. W. Shuai, Phys. Lett. A **285**, 312 (2001).
[24] V. Andrade, R. L. Davidchack, and Y. C. Lai, Phys. Rev. E **61**, 3230 (2000).
[25] I. Kim, C. M. Kim, W. H. Kye, and Y. J. Park, Phys. Rev. E **62**, 8826 (2000); J. Y. Chen, K. W. Wong, H. Y. Zheng, and J. W. Shuai, *ibid.* **63**, 036214 (2001); J. Y. Chen, K. W. Wong, and J. Y. Shuai, *ibid.* **12**, 100 (2002); W. H. Kye and C. M. Kim, *ibid.* **62**, 6304 (2000); Z. G. Zheng, B. B. Hu, and G. Hu, *ibid.* **62**, 402 (2000).